Poster #M236B

Tropical Intraseasonal Variability Simulated in the NASA GISS General Circulation Model

Daehyun Kim[1] (dkim@ldeo.columbia.edu), Adam H. Sobel[1,2,3], Anthony D. Del Genio[4], Yonghua Chen[2,4], Suzana J. Camargo[1], Mao-Sung Yao[4,5], Maxwell Kelley[6], and Larissa Nazarenko[6]

[1]Lamont-Doherty Earth Observatory of Columbia University, Palisades, NY, [2]Department of Applied Physics and Applied Mathematics, Columbia University, New York, NY, [3]Department of Earth and Environmental Sciences, Columbia University, New York, NY, [4]NASA Goddard Institute for Space Studies, New York, NY, [5]Sigma Space Partners, Institute for Space Studies, New York, NY, [6]Center for Climate System Research, Columbia University, New York, NY

The tropical intraseasonal variability simulated by the atmospheric model of the National Aeronautics and Space Administration (NASA) Goddard Institute for Space Studies (GISS) general circulation model (GCM) - Model_E is examined in this study.

Experimental Design

EXP	Description
AR4a	AGCM component of the AR4 version
AR5a	AGCM component of the AR5 version
AR5a_Ent1	Same as AR5, except for higher entrainment rate, without fraction constrain, one plume per each cloud base

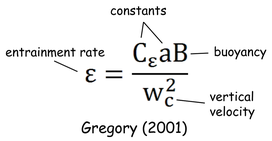

Wavenumber-frequency diagram

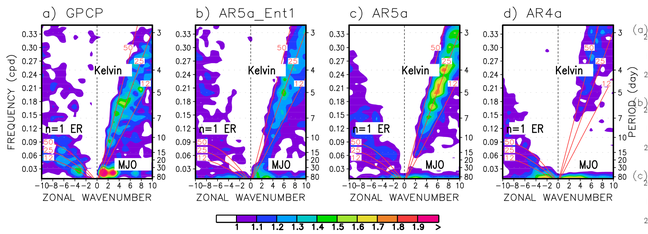

FIG. 1. Space–time spectrum of the 15°N–15°S symmetric component of precipitation divided by the background spectrum. (a) GPCP, (b) AR5a_Ent1, (c) AR5a, and (d) AR4a. Superimposed are the dispersion curves of the odd meridional mode numbered equatorial waves for the five equivalent depths of 12, 25, and 50m.

Mean and intraseasonal variability

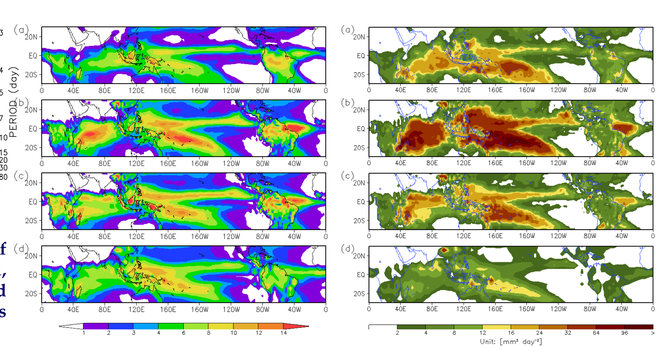

The new version of Model_E, which will be used for the Intergovernmental Panel for Climate Change (IPCC) 5th Assessment Report (AR5) shows clear improvements compared to the AR4 version in simulating the magnitude of intraseasonal variability, and the amplitude and phase speed of convectively coupled Kelvin waves. Despite these improvements, the AR5 version still lacks the Madden-Julian oscillation (MJO) mode, which dominates intraseasonal variability over the tropics and interacts with many other climate components in nature.

FIG. 2 (left). November–April mean precipitation (mm day^{-1}) of (a) GPCP, (b) AR5a_Ent1, (c) AR5a, and (d) AR4a

FIG. 3 (right). Variance of 20–100-day bandpass filtered precipitation (mm^2 day^{-2}) of (a) GPCP, (b) AR5a_Ent1, (c) AR5a, and (d) AR4a

Combined EOF

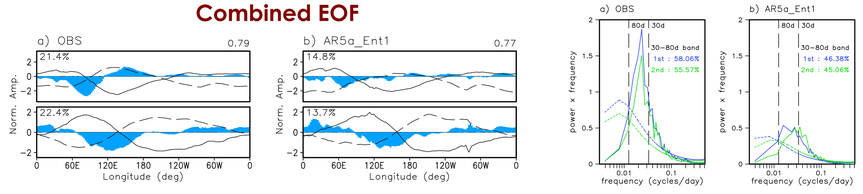

FIG. 4 (left). First two CEOF modes of 20–100-day 15°S–15°N averaged 850-hPa and 200-hPa zonal wind and OLR for the (a) NCEP/NCAR and AVHRR, (b) AR5a_Ent1. The total variance explained by each mode is shown in the lower left of each panel. The mean coherence squared between principal components of two modes within a 30–80-day period is given above the upper panel.

FIG. 5 (right). The power spectrum of the unfiltered PC derived by projecting the CEOFs onto unfiltered data (seasonal cycle removed): first mode (blue) and second mode (green). (a) NCEP/NCAR and AVHRR, (b) AR5a_Ent1. Dashed lines show the 99% confidence limit for a red noise spectrum.

The MJO is defined here as the leading mode of coherent variability between anomalies of upper and lower tropospheric zonal wind, and convection. Combined empirical orthogonal function (CEOF) approach (Wheeler and Hendon 2004) is adopted for this purpose. The CEOFs in AR5a_Ent1 capture the gross features of the leading mode in observations, such as the location of the maximum in convection (minimum OLR), baroclinic wind structure, and planetary spatial scale. The power spectrum of the unfiltered PC shows that the MJO extracted by CEOF has spectral peaks near observed MJO time scale that are physically meaningful and distinct from a red noise process.

MJO life-cycle composite

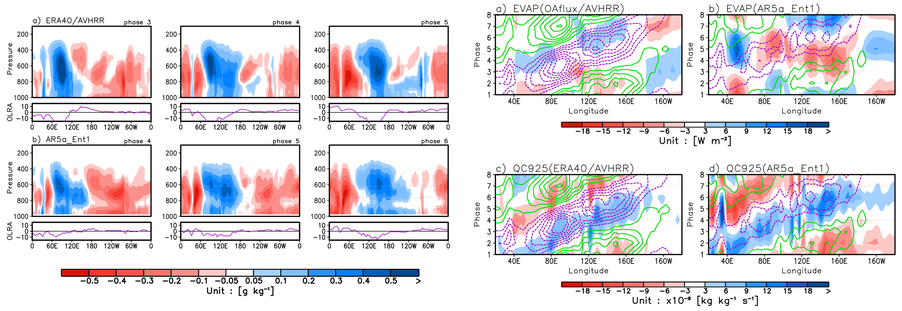

FIG. 6 (left). MJO life-cycle composite of 20-100 day bandpass filtered, 10°S-10°N averaged specific humidity anomaly (upper panel), and filtered, 10°S-10°N averaged OLR anomaly (lower panel) at different phases in which the convective anomaly is located near the Indian Ocean and Maritime continent. a) ERA40/AVHRR, and b) AR5a_Ent1

FIG. 7 (right). Phase–longitude diagram of OLR [contour plotted every 3 W m^{-2}, positive (green) and negative (purple)] and 925-hPa moisture convergence (kg kg^{-1} s^{-1}, upper)/evaporation (W m^{-2}, lower). (a), (c) Observations, and (b), (d) AR5a_Ent1. Phases are from MJO life cycle composite and values averaged between 10°S and 10°N.

As consistent with previous studies, simulation fidelity of the MJO strongly depends on cumulus parameterization. When the convective scheme is tuned to have greater entrainment, the AR5 version of Model_E simulates precipitation variability with spatial and temporal scales of the MJO. The MJO life-cycle composites of outgoing longwave radiation, evaporation, 925-hPa moisture convergence, specific humidity shows that the simulated MJO has realistic features. In observations and AR5a_Ent1, positive moisture anomalies in the lower troposphere develops ahead (east) of convective anomaly related to the MJO. Anomalous 925hPa moisture convergence leads convective anomaly, suggesting its role in moistening of the lower troposphere.

Re-initialization experiment

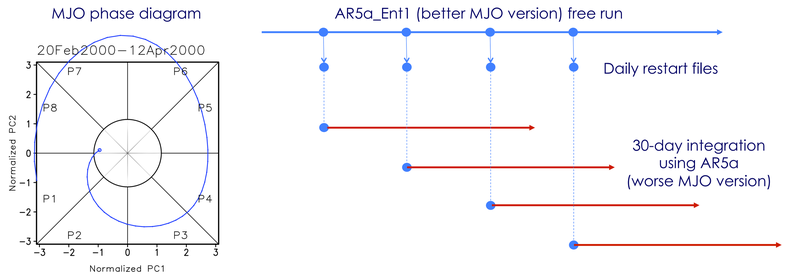

FIG. 8 (left). Hovmuller diagram of 15°S-15°N averaged precipitation during a strong-MJO period selected based on MJO phase diagram. a) AR5a_Ent1, b) 10-day and c) 20-day after reinitialization, and d) AR5a.

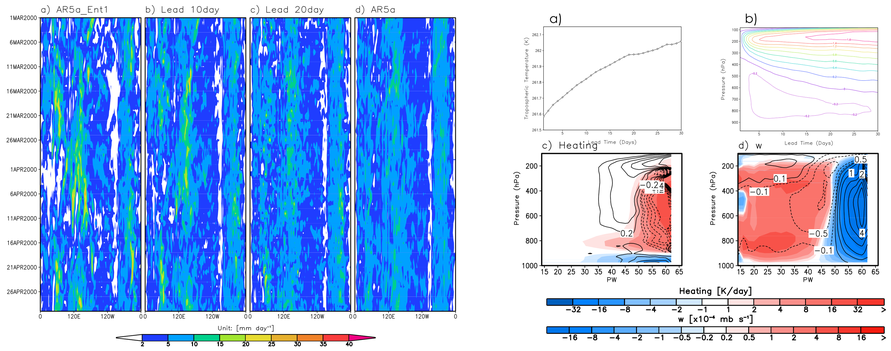

FIG. 9 (right). a) Tropics-averaged tropospheric temperature during the 30-day integrations. b) Pressure-lead time plot of deviation temperature from the first day-mean. Composited c) diabatic heating rates and d) pressure velocity of the AR5a_Ent1 simulation (shaded) based on precipitable water. Contours in c) and d) show the first-day deviation of the re-initialization experiment from AR5a_Ent1.

By re-initializing relatively poor-MJO version with restart file from relatively better-MJO version, a series of 30-day integration is performed to examine the impacts of the parameterization changes on the organization of tropical convections. The results show that the poor-MJO version with smaller entrainment rate has a tendency to reduce the contrast between dry and wet regimes, thereby the tropical convections become less organized and diffusive.

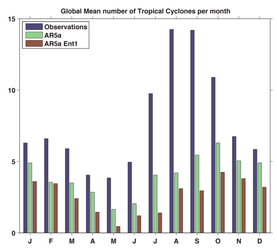

MJO vs. Tropical cyclone

FIG. 10. Number of tropical cyclones (NTC) per month globally. Blue: Observations, Green: AR5a, and Red: AR5_Ent1.

The statistics of tropical cyclones (e.g. number) in the model are also affected by the changes in convection scheme. With the larger entrainment rate, the model simulates a smaller number of tropical cyclones. Our results suggest that modeling entrainment rate in convection scheme is crucial in the simulation of the tropical ISV, such as the MJO and tropical cyclones.